WILEY-VCH

DOI: 10.1002/ ((please add manuscript number))
Article type: Full Paper

Hot Electron Based Solid State TiO_2|Ag Solar Cells

Hannah-Noa Barad, Adam Ginsburg, Hagai Cohen, Kevin J. Rietwyk, David A. Keller, Shay Tirosh, Yaniv Bouhadana, Assaf Y. Anderson, and Arie Zaban**

H.N. Barad, A. Ginsburg, Dr. K.J. Rietwyk, D.A. Keller, Dr. S. Tirosh, Dr. Y. Bouhadana, Dr. A.Y. Anderson, Prof. A. Zaban
Department of Chemistry, Center for Nanotechnology & Advanced Materials, Bar Ilan University, 5290002 Ramat Gan, Israel.

E-mail: assaf.anderson@gmail.com, arie.zaban@biu.ac.il

Dr. H. Cohen
Department of Chemical Research Support, Weizmann Institute of Science, 76100 Rehovot, Israel.

Keywords: plasmonics, combinatorial materials science, high-throughput, nanoparticles, photovoltaics

Abstract:

The present work reports a simple and direct sputtering deposition to form solid state TiO_2|Ag independent plasmonic solar cells. The independent plasmonic solar cells are based on a Schottky barrier between two materials, TiO_2 and Ag. The Ag functions as the absorber generating 'hot' electrons, as well as the contact for the solar cell. The Ag sputtering is performed for different durations, to form Ag nanoparticles with a wide size distribution on the surface of rough spray pyrolysis deposited TiO_2. IPCE measurements show photovoltaic activity below the TiO_2 bandgap, which is caused by the silver nanoparticles that have a wide plasmonic band, leading to the generation of 'hot' electrons. X-ray photoelectron spectroscopy analysis

supports the 'hot' electron injection mechanism by following the Ag plasmon band, and detecting local photovoltages. The measurements show that electrons are formed in the Ag upon illumination and injected into the TiO_2, to produce photovoltaic activity. J-V measurements show photocurrents up to 1.18 mA cm^{-2} and photovoltages up to 430 mV are achieved with overall efficiencies of 0.2%. This is, to our knowledge, the highest performance reported for such independent plasmonic solar cells.

1. Introduction

Plasmonic solar cells, which are one of the presently researched photovoltaic systems,[1] contain metallic nanoparticles that are utilized for electron generation or for light trapping and scattering in the solar cells. The importance of the plasmonic effect on photovoltaics is that it improves basic processes within solar cells such as electron generation and injection, charge separation, and reducing recombination. The presented research focuses on plasmonic photovoltaics as absorbers for generating and injecting electrons, unlike most of the research in the plasmonic solar cell field. The basic operation of the discussed solar cells, including formation of charge carriers, is due to the plasmonic effect in the cells, and is not just supported or enhanced by it.

The operation of plasmonic solar cells is dependent upon the optical excitation of surface plasmons, which are collective oscillations of the surface electronic cloud in metallic nanoparticles. One of the important characteristics of metallic nanoparticles is the coupling interaction of their plasmonic oscillations with incident photons of the same frequency; this coupling excites surface plasmon resonance (SPR).[1] The SPR gives rise to strong electromagnetic fields, which can be used for trapping or reflecting light, enhancing photovoltaic activity,[2] surface-enhanced Raman spectroscopy (SERS),[3] and photo-catalysis.[4] When the

surface plasmon decays to the ground state it can cause electron excitation within the metallic nanoparticle itself, the excited electrons are often referred to as 'hot' electrons. The 'hot' electrons are highly active non-equilibrium electrons that have sufficient kinetic energy to overcome potential barriers, or tunnel through thin layers of semiconductors.[5] Since the 'hot' electrons are energetic they can be used in conjunction with a semiconductor, to form a Schottky barrier photovoltaic device. As the absorption and excitation of the SPR is very wide and extends beyond the visible range of the solar spectrum, depending on the material and structure, the 'hot' electrons that are formed can extend the spectral response of the photovoltaic device. The 'hot' electrons are directly injected into the conduction band of the semiconductor, forming and improving the photovoltaic activity.

One of the semiconductors that is used extensively for renewable energy applications is TiO_2, which is a wide bandgap (3.2 eV) metal oxide semiconductor. As it is a highly n-type material, it is utilized namely as an electron conducting layer in solar cells to help with charge separation,[6] or as a photocatalyst for water splitting.[7] The wide bandgap of the TiO_2 only allows it to be used for solar cells in conjunction with an absorbing material, be it dye, quantum dots, or other materials, since by itself it would only absorb light from the UV part of the solar spectrum. To improve or form the photovoltaic activity of the TiO_2 as an independent photovoltaic system, silver metallic nanoparticles or nanostructures can be used. The metallic nanoparticles form a Schottky barrier solar cell with the TiO_2, and the 'hot' electrons that have enough kinetic energy to overcome the Schottky barrier height are injected into the TiO_2, as can be seen in the schematic depiction of the mechanism in **Figure 1**. The 'hot' electron injection from the Ag nanoparticles into the TiO_2 leads to charge separation and photovoltaic activity. Furthermore,

since the Ag nanoparticles absorb light in the visible region, they are capable of increasing the absorption of the TiO_2 and hence the performance of a TiO_2|Ag independent plasmonic solar cell.

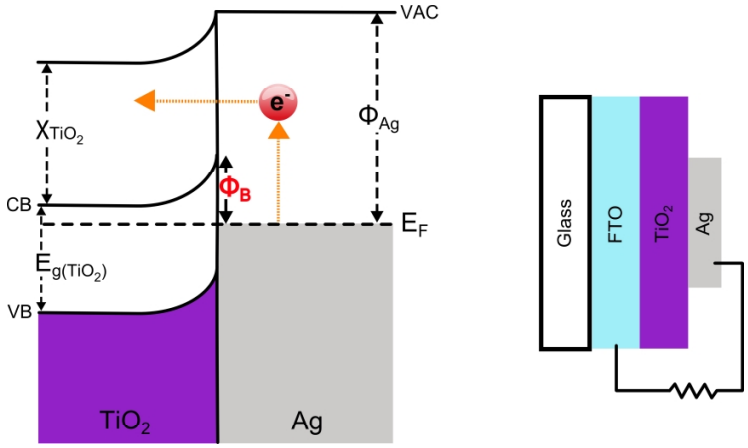

Figure 1. The left side shows a schematic depiction of a Schottky barrier solar cell formed between TiO_2 and an Ag nanoparticle, where VAC is the vacuum energy level, Φ_{Ag} is the work function of the Ag nanoparticle, Φ_B is the Schottky barrier height, and χ_{TiO2} is the electron affinity of the TiO_2. In the proposed mechanism, the decaying SPR excites 'hot' electrons in the Ag nanoparticles that possess enough energy to overcome the Schottky barrier, and inject into the TiO_2, forming a photocurrent. The oxidized silver must be regenerated in order to continue the solar cell operation. The regeneration is achieved by a hole transport material or a conductive contact. The right side represents a schematic diagram of the solar cell structure, which contains two components (besides the substrate), TiO_2 and Ag.

A disadvantage of plasmonic solar cells is the complicated deposition methods of the metallic nanoparticles.[8] That is, synthesizing the Ag nanoparticles is not always simple and straightforward; usually control of the solution and environment are needed, as well as various capping agents to stabilize the nanoparticles.[7, 9] Furthermore, in order to achieve a desired set plasmonic modes, specific shapes must be fabricated, such as nanorods (for photocataltysis),

which complicates device fabrication.[8b] Moreover, to improve photocatalytic or photovoltaic characteristics, especially in organic photovoltaics, Ag nanoparticles have to be embedded within or between the active layers.[8c] In order to form these Ag nanoparticles within the active layers, templates, nanolithography, or nanofabrication techniques are required.[8a] The fabrication methods that are used are complex, time consuming, and not always suitable for photovoltaic applications. Consequently, it is necessary to find simple and direct deposition methods to form the metallic nanoparticles in order to achieve low cost plasmonic solar cells. Nonetheless, Ag nanoparticles have recently been used with TiO_2 as light trapping and light reflecting agents, as well as electron-hole recombination suppressors, to improve the photovoltaic performance of dye sensitized solar cells (DSSC),[10] quantum dot sensitized solar cells,[11] and hybrid polymer solar cells.[12]

The use of Ag nanoparticles as the active absorbing layer with TiO_2 for independent plasmonic solar cell applications was proposed by Tian *et al.*,[13] who demonstrated plasmon-induced photoelectrochemistry of non-porous TiO_2 decorated with Ag and/or Au nanoparticles. Incident photon to current efficiency (IPCE) of ~4% was achieved for TiO_2 decorated with Ag nanoparticles, measured in a NaOH aqueous solution. In another investigation, glutathione protected silver and gold nanoclusters were used to sensitize TiO_2 in the same setup as DSSCs, using an electrolyte and Pt counter electrode.[14] The Ag nanocluster sensitized solar cell gave a short circuit current of ~40 μA cm^{-2} and an open circuit voltage of 270 mV, while the Au-Ag composite nanocluster solar cell gave higher performances. Other work showed the synthesis of Ag nanoparticle and TiO_2 composite thin films, which obtained photocurrents of ~20 μA cm^{-2}. In this study the photoelectrochemical mechanism that was proposed involved SPR photo-excited electrons, which were injected into the TiO_2 conduction band.[15]

In all the investigations mentioned above there is always use of an electrolyte and the solar cell structure is photoelectrochemical. As the Ag nanoparticles inject a 'hot' electron into the TiO_2 conduction band, the Ag becomes oxidized, and is left with a hole (positively charged).[16] The Ag nanoparticle is reduced back to its original state by electrons from the electrolyte in the wet electrochemical setup. However, efforts have been made to turn the TiO_2 and Ag nanoparticle solar cell into a solid state device. Takahashi *et al.* [17] used an Al_2O_3 nano-mask to deposit Ag nanoparticles on top of a TiO_2 layer on one side, and deposited indium tin oxide (ITO), which served as the conductive layer on the other side of the nanoparticles, achieving an IPCE of ~0.6%. More recently, Reineck *et al.*[18] prepared solar cells by self-assembly of 25 nm Ag nanoparticles on TiO_2, with Spiro-OMeTAD as the hole conducting layer on top of the Ag particles. Using accelerated lifetime testing (under 505 nm LED illumination) an average photocurrent of ~550 μA cm^{-2} was demonstrated. In both of the aforementioned cases no current density-voltage (J-V) curves were given to support the photovoltaic activity of the cells.

In the present research, we show that 'hot' electrons are generated in silver nanoparticles that spontaneously form during sputtering on TiO_2, prepared by spray pyrolysis. The formation of the Ag nanoparticles, which have a large size distribution, is achieved without complicated deposition techniques, and is due to the rough nature of the TiO_2 layer. The method used in the investigation is the combinatorial material science approach, which utilizes combinatorial fabrication methods and high-throughput characterization tools. Combinatorial material science has been used in the past to investigate electronic materials, new magnetic materials, catalysts,[19] and solar cells,[20] but has not been used to study plasmonic based solar cells, and specifically TiO_2|Ag independent plasmonic solar cells. To investigate these solar cells, the silver was deposited with different thicknesses using radio frequency (RF) sputtering. We characterize the

resulting TiO_2|Ag independent plasmonic solar cells using a combination of photoemission and combinatorial techniques. The former is used to confirm the 'hot' electron mechanism for generation of the photoactivity and to develop a band diagram of our solar cells. The 'hot' electron mechanism in the solid state TiO_2|Ag solar cell is regenerative, and can operate in a closed circuit without the addition of a hole-transporting material. We utilize J-V measurements to show how the performance of our solar cells varies with Ag deposition times. Using IPCE measurements we provide evidence that the 'hot' electron mechanism is supported by an enhancement of the photoresponse of the solar cells into the visible region of the solar spectrum. The best cell performances give short circuit currents up to 1.18 mA cm^{-2} and open circuit voltages up to ~400 mV, with efficiencies of 0.2%. To our knowledge, the obtained photocurrents are much higher than any reported for TiO_2|Ag independent plasmonic solar cells so far.

2. Results and Discussion

The plasmonic solid state TiO_2|Ag independent solar cells were studied with a combinatorial approach. **Figure 2** shows the schematic configuration of a combinatorial library with varying thicknesses of TiO_2 and thicknesses of the silver. Initially, a linear thickness gradient of TiO_2 was deposited using spray pyrolysis. Then, the Ag was sputtered for different durations through a shadow mask with a 13×13 grid of round holes onto the library, where each row has a different thickness. The resulting library contained 169 solar cells differing from each other by their TiO_2:Ag ratio. Each of the cells in the library was characterized using high-throughput techniques.[21] Figure S5b in the Supporting Information, shows the thickness of the TiO_2 as analyzed by the optical measurements. The thicknesses of the Ag points were estimated based on

the sputtering parameters, and are shown in **Table 1** (experimental section). The first row (numbered 1) has the least amount of Ag, and the amount of Ag increases with each row.

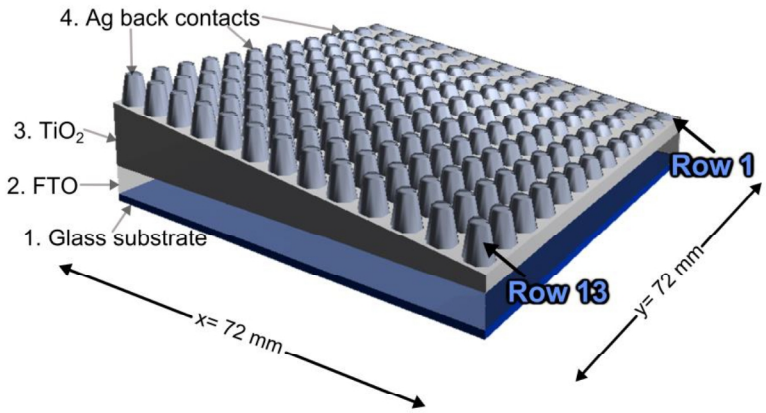

Figure 2. Schematic of the structure of the studied library containing 169 separate solar cells. The TiO_2 layer was deposited as a linear gradient by spray pyrolysis on a glass slide (72 mm x 72 mm) coated with FTO layer (transparent conductive oxide). The Ag is deposited on top of the TiO_2 layer by sputtering, using a shadow mask with 169 holes. The thickness changes of the TiO_2 and Ag layers are indicated in the scheme. The TiO_2 is thickest on the left side of the library, with a linear decrease in thickness to the right side of the library (Figure S5b, Supporting Information). The Ag has the lowest thickness in row 1 (shortest deposition time) with the highest thickness being in row 13 (longest deposition time). The Ag forms as thin nanoparticle films, and the cones are only used to depict the different thicknesses.

The SPR occurs in metallic nanoparticles, and as such it is critical that the silver nanoparticles are in the metallic Ag^0 state, and not in one of the oxidized states. In order to rule out the formation of silver oxides in the silver patches and check that the Ag does not penetrate into the

TiO_2, X-ray photoelectron spectroscopy (XPS) and Rutherford Backscattering (RBS) were performed. Bare TiO_2 and points with Ag film thicknesses of 10 and 100 nm, rows 2 and 10, respectively, were measured by XPS, as seen in **Figure 3**. Figure 3a presents XPS results for the Ti 2p core level. The Ti $2p_{3/2}$ peak position is 459.24 eV representing the Ti^{+4} oxidation state, as expected for TiO_2.[22] The binding energy of the Ag $3d_{5/2}$ core level is 368.30 eV (Figure 3b), indicative of the Ag^0 metallic state. The peak positions for oxidized silver, being mainly AgO or Ag_2O, have been reported for binding energies of 367.8-368 eV and 367.3-367.6 eV, respectively,[23] hence there is probably a small amount of oxidized Ag in the library, and only on the top surface, no other Ag species (such as sulfides) were seen at all. The inset in Figure 3b shows a widespread plasmonic peak for the silver, as a function of its energetic distance from the Ag $3d_{5/2}$ peak. The plasmonic peak, which also supports that metallic silver was obtained, ranges from binding energies of 370.6 eV to 372.8 eV (distance from Ag $3d_{5/2}$ peak is 2.3 eV to 4.5 eV). The energy of the surface plasmon peak depends on the size and shape of the silver nanoparticles from which it arises. Notably, the corresponding XPS signal is broad, with a pronounced extension to low energies, as compared to the typical bulk plasmon of silver at 3.8 eV. Therefore this broad XPS signal reflects the presence of a broad band of plasmonic modes, which is typical to nanoparticles in general and, possibly, also to the size and shape distribution of these nanoparticles.

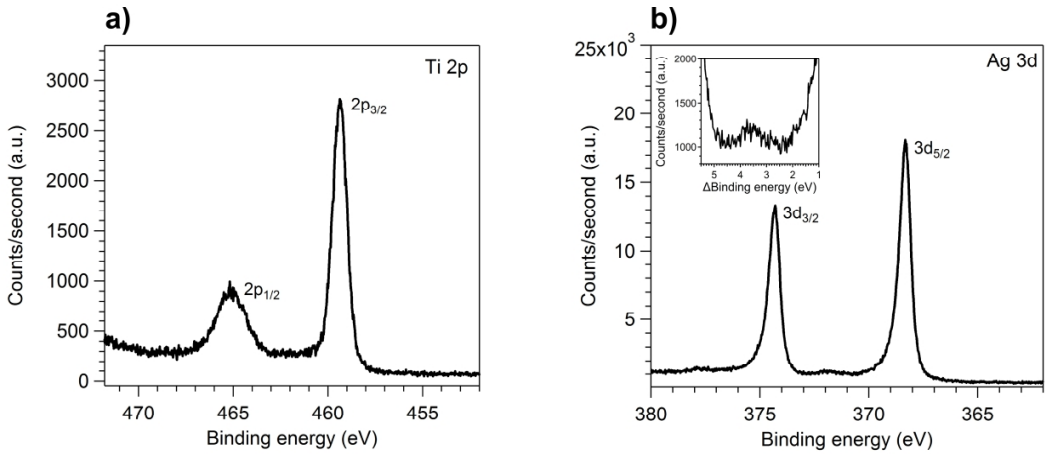

Figure 3. XPS results show the silver on the surface of the TiO_2 probably did not oxidize. **a)** Binding energy Ti 2p core level. The Ti $2p_{3/2}$ peak position at 459.37 eV indicates the Ti^{+4}, supporting the formation of TiO_2. **b)** Binding energy of Ag 3d core level. The Ag $3d_{5/2}$ peak position is 386.3 eV, which confirms that metallic Ag^0 is formed and no silver oxides are seen. RBS measurements given in Figure S1 (Supporting Information), further confirm the Ag films are metallic. The inset shows the broad Ag plasmonic peak. The widespread peak suggests that there are many plasmonic modes in the Ag film, meaning that the silver layer is constructed of nanoparticles with different sizes and shapes.

To further confirm the existence of Ag and to check if the Ag penetrates into the TiO_2 film, RBS measurements were performed (Figure S1, Supporting Information). The results for the RBS measurements show a sharp surface peak for the Ag that does not overlap with the TiO_2 layer beneath it, meaning that there is no penetration of Ag into the TiO_2 layer and that the silver at the TiO_2-Ag interface did not oxidize. Moreover, composition calculations show 100% of silver atoms for the surface peak and no indication to the presence oxygen atoms, signifying that the

Ag is probably metallic, although the presence of an oxidized layer on top of the surface of the Ag patches is not completely ruled out.

The library was measured by high resolution scanning electron microscopy (HRSEM), and cross sections were prepared and measured by a focused ion beam scanning electron microscope (FIB-SEM) to determine the structural surface and cross sectional morphology of the TiO_2 and Ag films. As can be seen in the top left of **Figure 4**, the surface of the bare TiO_2 layer is very rough (~50-60 nm variations), which is due to the spray pyrolysis deposition method, following the FTO surface roughness. The Ag nanoparticles, which form on the TiO_2 layer, have a wide size distribution (Figure S3, Supporting Information), and form preferentially on the sides and edges of the TiO_2, which may represent high energy TiO_2 atomic planes, that favor the Ag deposition.[24] The TiO_2 surface roughness and structuring can explain the formation of the Ag nanoparticles, as shown in the top right of Figure 4, for the 60 second deposition time (15 nm). The nanoparticles spontaneously form during the sputtering deposition on the rough surface of the TiO_2, and are not homogeneous in size or shape and do not completely cover the TiO_2 surface. Energy-dispersive X-ray spectroscopy (EDS) measurements, shown in Figure S2 and Table S1 (Supporting Information), were performed to check for the presence of Ag on the TiO_2 coated with the nanoparticles. The produced silver nanoparticles confirm the assumption that the broad Ag plasmonic peak, observed in the XPS measurements, is due to the many plasmonic modes originating from the variety in size and shape distribution of the Ag nanoparticles. When increasing the deposition time further to 480 seconds (120 nm, Figure 4 bottom left), a thin layer of the Ag is formed. This layer is still comprised of nanoparticles, and has a nanostructured and rough nature, due to the surface structuring of the TiO_2, as can be seen in the cross section FIB-SEM image (Figure 4 bottom right). The cross section shows that the silver morphology is

dictated by the surface roughness of the TiO_2 layer. As such, when small amounts of Ag are deposited, nanoparticles form on the TiO_2, and when large amounts of Ag are deposited, nanostructured thin films are formed. These results indicate that it can be simple to pattern nanoparticle on a rough surface, using direct deposition methods such as sputtering.

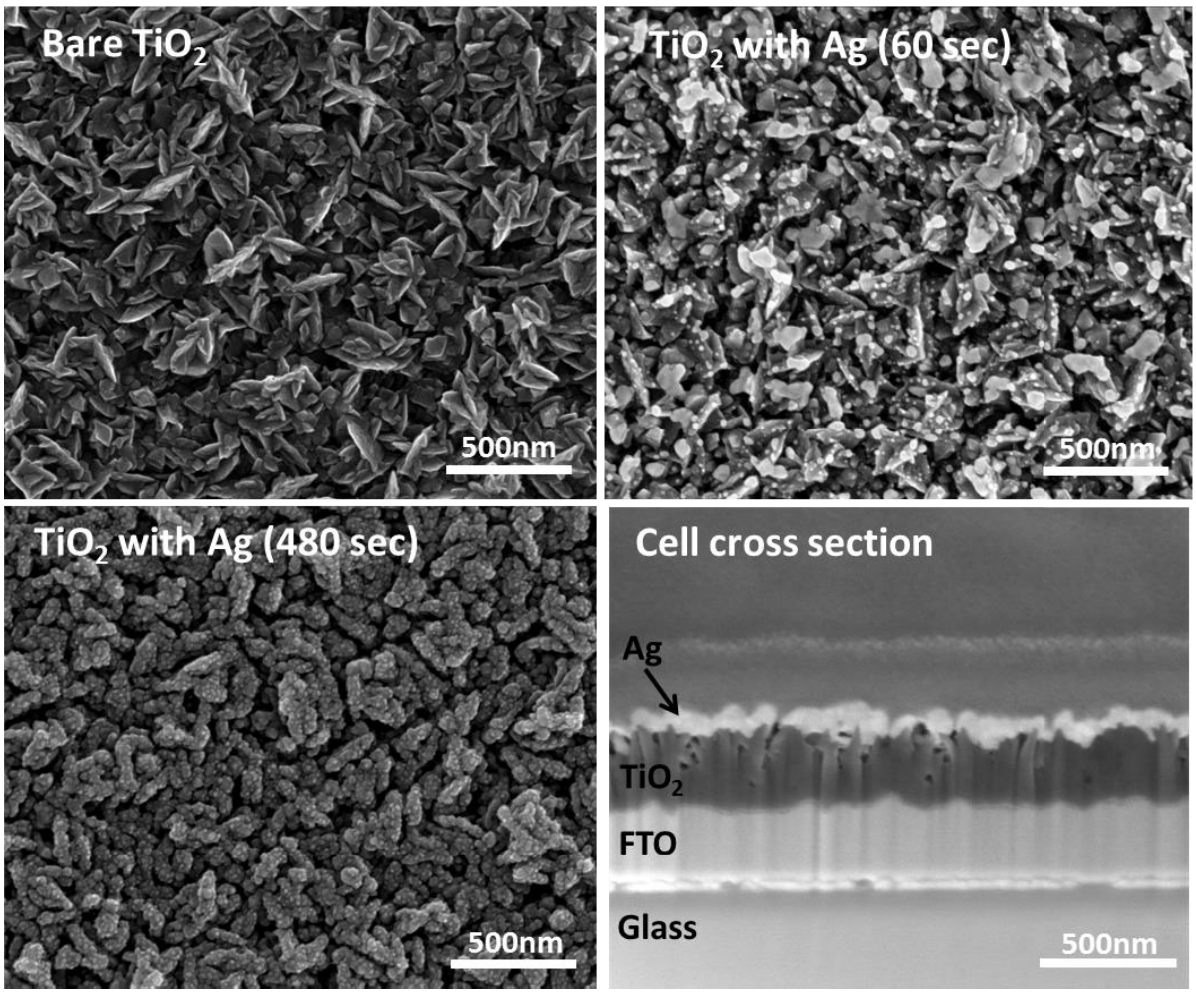

Figure 4. Surface HRSEM and cross section FIB-SEM micrographs of: Bare TiO_2, TiO_2 with 60 seconds deposition of Ag, TiO_2 with 480 seconds deposition of Ag, and a cross sectional cut of the 480 seconds point. The bare TiO_2 is highly rough leading to formation of nanoparticles and nanostructured thin films of Ag, in a simple direct way.

For photovoltaic analysis the J-V characteristics of the library were measured. There is high photovoltaic activity for the library, given that the absorber materials are small metallic nanoparticles on the surface of the TiO_2. As shown in the photovoltaic maps in **Figure 5**a, the short circuit currents (J_{sc}), open circuit voltages (V_{oc}), fill factors (FF), and maximum powers (P_{max}) all increase with Ag deposition time up to 480 s (120 nm, row 12, Figure 2). In Figure 5a Short circuit currents of up to 750 μA cm^{-2}, and open circuit voltages of 430 mV are achieved. The FFs exceed 60% and the P_{max} reaches 100 μW cm^{-2}. The increase of the photocurrents, as a function of Ag deposition time (nanostructured Ag film thickness), is caused either by the higher amount of absorbing material or by the fact that the particles start connecting to each other at higher deposition times. When there is more silver, a larger amount of SPR occurs, leading to more 'hot' electrons being generated and injected into the TiO_2. While the higher deposition times also lead to better interconnections between Ag nanoparticles and hence better conductivity, there is also much more SPR in the thick Ag layers that is the main contributor to the better performance in these thicknesses. It is highly probable that since the Ag nanoparticles in the shorter deposition times have almost no interconnections between them that the conductivity is low. The low conductivity issue in the thinner Ag adds to the lower photovoltaic activity, in parallel to the fact that the lower Ag deposition times also have less SPR in general, leading to formation of less `hot` electrons. In a separate deposition of 400 s (100 nm) of Ag on TiO_2, short circuit currents of 1.18 mA cm^{-2}, and open circuit voltages of ~380 mV are attained (Figure 5b). The energy conversion efficiency (η) of this solar cell is 0.2%, which is the highest efficiency that has been achieved, as far as we know, for a solid state TiO_2|Ag independent Schottky barrier plasmonic solar cell. These results are particularly interesting considering no hole transport layer was introduced in the solar cells, and they are manufactured in a simple

direct method, removing the nessecity of special templating or lithography steps needed to form the nanoparticles. Using a direct method as sputtering for depositing the Ag naoparticles is also important for better contact between the Ag nanoparticles and the TiO_2 layer, since it is performed under vacuum, thus providing a very clean and contamination free enviornment. Sputtering also removes the need for capping and stabilizing agents around the Ag nanoparticles, which are essential in wet chemical synthesis methods, improving the conductivity and electrical contact to the TiO_2 layer. Another advantage to using sputtering is that masks made out of avaiable materials (i.e. Aluminium or stainless steel) can be used, multiple times, to easily form patterns where the Ag nanoparticles can be deposited. Additionally, the sputtering technique is highly controllable; thicknesses, as an example, can be readily determined during the deposition, which is not the case for wet chemical synthesis methods.

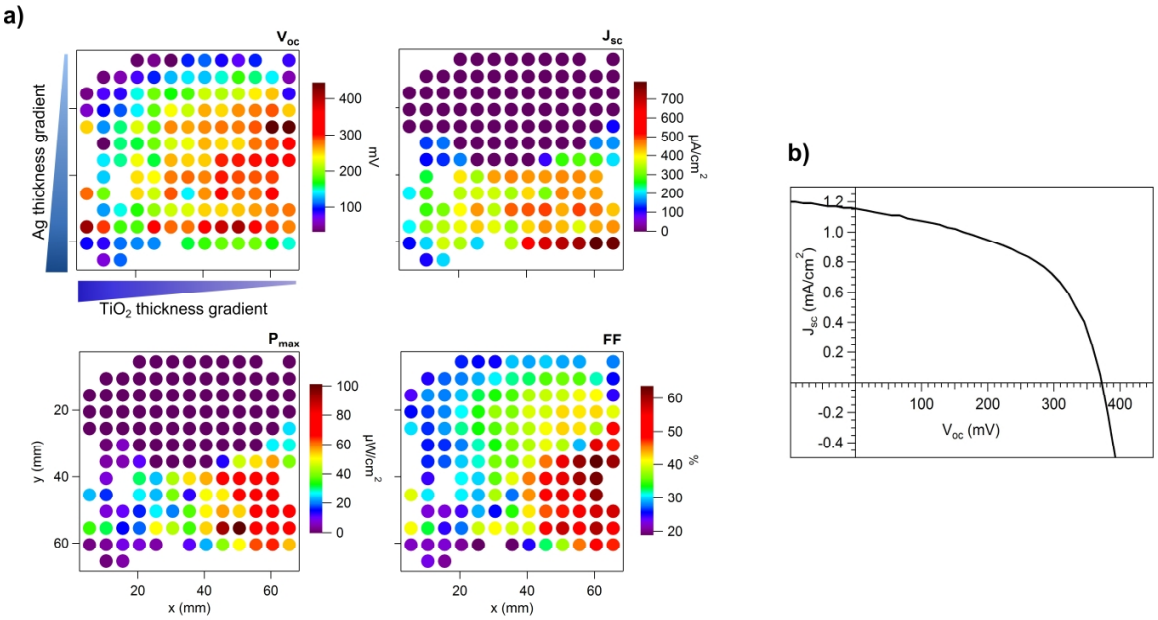

Figure 5. a) J-V characteristics color maps for the TiO_2|Ag plasmonic solar cells, clockwise from top left: V_{oc}, J_{sc}, FF, and P_{max}. The TiO_2 linear gradient thickness and the Ag gradient thickness are indicated next to the V_{oc} map. The results show photovoltaic activity throughout

the library for all TiO_2 and Ag thicknesses. Areas that have no dots (or white dots), were not considered as photovoltaic and were not analyzed. **b)** J-V curve of best TiO_2|Ag solid state solar cell prepared separately on TiO_2 with an Ag deposition time of 400 s (100 nm calibrated thickness). The photocurrents reach up to 1.18 mA cm^{-2}, which are the highest reported for TiO_2|Ag solar cells as far as we know.

To determine the source of the photovoltaic activity, the IPCE of several cells in the TiO_2|Ag library were measured (**Figure 6**) along the center column of the library (Figure 2). The results clearly indicate a peak corresponding to the Ag nanoparticle SPR band ranging from 400-450 nm (Figure 6a), with an onset at ~700 nm. This SPR active band does not belong to the TiO_2 as its optical absorption onset starts at about 380 nm. The peak seen between 400-450 nm, with an onset at 700 nm, corresponds very well with the range of plasmonic energies that are observed by XPS (inset Figure 3b). Similar IPCE peaks, at about 460 nm with an onset at ~600 nm, have been seen in the past for self-assembled Ag nanoparticles on TiO_2.[18] In that research the nanoparticle diameters were in between 10 to 50 nm, with an average diameter of 25 nm. Whereas here, the rough surface of the TiO_2 enables the formation of silver nanoparticles with various sizes and shapes. The smallest Ag particle diameters are less than 5 nm, while the largest nanoparticles reach sizes of ~500 nm (Figure S3, Supporting Information). The large size variation, between the Ag nanoparticles is probably the cause of the wide IPCE active range, from 400 to 700 nm. The IPCE values increase with the size of the Ag nanoparticles and reach 1.4%. The higher IPCE values for the larger Ag thicknesses confirm that when there are more plasmonic absorbers in the solar cells then more 'hot' electrons are formed, leading to better photovoltaic performance, which is seen in the J_{sc} results (Figure 5a). Further evidence for the

role of surface plasmons is provided by the fact that the IPCE peak shifts towards longer wavelengths as the thickness of the Ag (based on deposition time and rate) increases (Figure 6b). The particle size analysis, seen in Figure S3, shows an increase in the general size as the deposition time grows. Thus the IPCE peak shift is attributed to the growth in the average sizes of the nanoparticles with increase of the Ag deposition time, and is verified in two different libraries (prepared using the same methods). According to the Mie theory there is a red shift of plasmonic absorption of nanoparticles as they increase in size,[25] supporting the observed results.

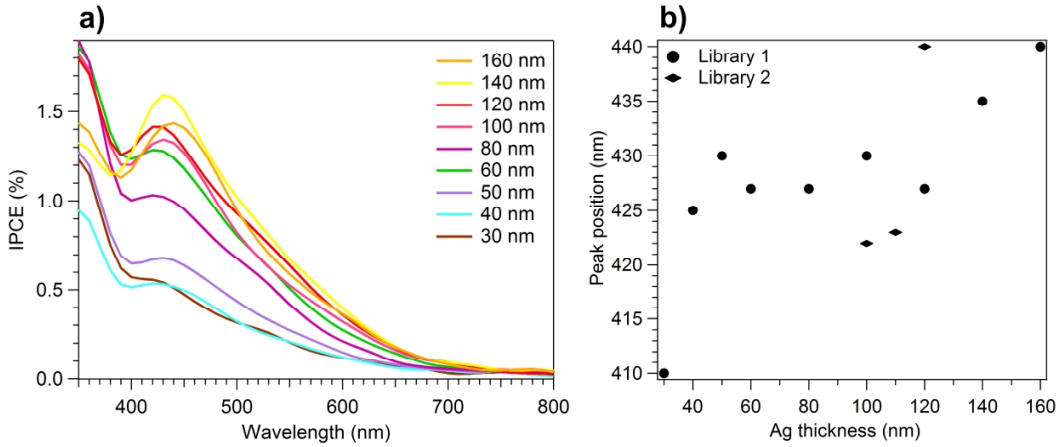

Figure 6. a) IPCE spectra of different thicknesses of Ag deposited on TiO_2. The spectra show an active peak between 400-450 nm, attributed to the plasmonic absorption of the Ag nanoparticles. **b)** Peak positions *vs.* the Ag thickness, for two different libraries, showing a red shift in the peak position at higher Ag thicknesses, contributing more evidence for the formation of SPR, which results in the photovoltaic activity.

To further confirm the 'hot' electron injection mechanism behind the photovoltaic activity, XPS-based chemically resolved electrical measurements (CREM)[26] were performed. The measurements were conducted under dark conditions, and then under illumination of a halogen

lamp. By evaluating the line shifts we could then learn about the local changes in electrostatic potential[26a, 27] and, importantly, compare the values extracted for the silver and TiO_2. The photo-response of the Ag $3d_{5/2}$ peak, given in **Figure 7**a, shows good reversibility of the Ag line shift, indicating that the photovoltage developing at the silver is nearly free of an irreversible drift component. A small shift in binding energy under illumination can be seen for the Ag $3d_{5/2}$ line. The Ag $3d_{5/2}$ peak shifts towards lower binding energies, which signifies that the Fermi energy level shifts downwards. The increase in the Fermi energy, relative to the vacuum level, upon illumination is caused by electrons being removed from the silver nanoparticles. The 'hot' electron injection from the Ag into the TiO_2 causes the Fermi energy in the silver to shift down from the vacuum level as it is losing electrons; hence the XPS results show lower binding energies for the Ag when it is illuminated. The corresponding Ti shift is found to be in the same direction (shifting to lower binding energies) although at a higher magnitude (~150 meV), thus the change in the Ag charging is positive relative to the TiO_2. Therefore, the overall effect is that of electrons going from the Ag into the TiO_2, leaving the latter surface negatively charged and the former positively charged. It is important to note that the spectrum of the halogen lamp has very low intensities up to ~550 nm; and the highest intensity of the halogen lamp is around 800 nm.

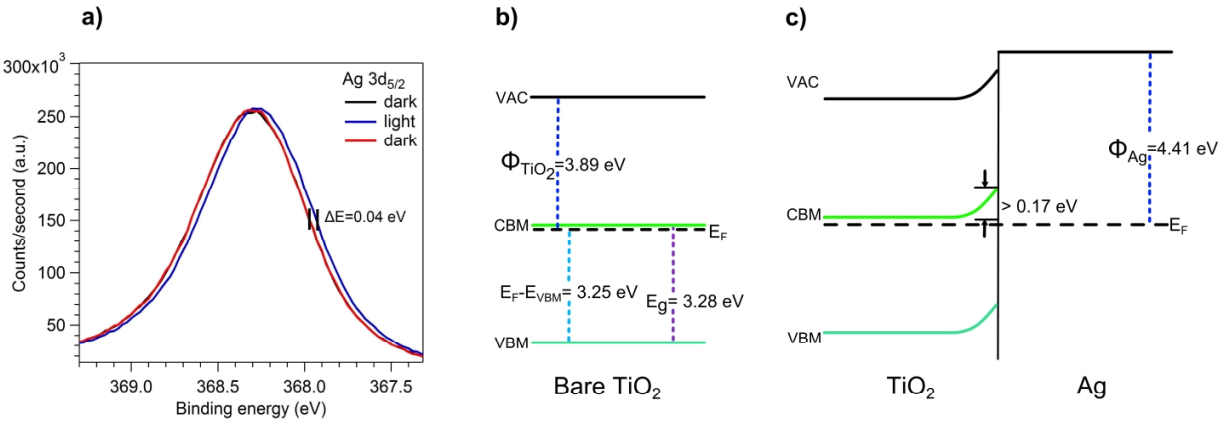

Figure 7. a) XPS measurements of the Ag $3d_{5/2}$ core level, under dark conditions and under halogen lamp illumination, where both dark measurements overlap exceedingly well (black and red curves). The results show a shift of the Ag $3d_{5/2}$ core level peak under illumination to lower binding energies, indicating an increase in the Fermi energy when the Ag is illuminated. The increase in Fermi energy shows that electrons are injected from the Ag into the TiO_2 upon illumination. **b)** Energy band diagram of the bare TiO_2 library, showing that the TiO_2 is highly n-doped. **c)** Energy band alignment diagram of the TiO_2|Ag solar cell. The TiO_2 has a band bending that is larger than 170 meV, which corresponds to the V_{oc} values that are achieved. Both the measured energy band alignment and the TiO_2 band bending support the 'hot' electron injection mechanism that is purposed.

A schematic presentation of the proposed energy band diagrams as derived for bare TiO_2 and for the TiO_2|Ag independent plasmonic solar cell is shown in Figure 7b-c. The band diagrams are based on XPS measurements given in Figures S4, and bandgap calculations[21] given in Figure S5a (Supporting Information). The TiO_2 bandgap was taken as 3.28 eV, which is an average value of all the points in the library (Figure S5a). For bare TiO_2 (Figure 7b), the energy separation of the Fermi level (E_F) and of the valence band maximum (VBM), E_F-E_{VBM}, is 3.25

eV, in agreement with previous reports.[28] The energy separation places the Fermi level ~0.03 eV below the conduction band minimum (CBM) for the bare TiO_2, indicative of a highly n-doped TiO_2 layer. In Figure 7c, the energy band alignment of the TiO_2|Ag independent plasmonic solar cell is presented. We used the measured work function of the 100 nm Ag cells as the work function of the Ag, since at this Ag thickness the TiO_2 is completely covered by the nanostructured Ag film. The Ti core level spectra of the bare TiO_2, and after the deposition of 10 nm reveal a binding energy shift average of 170 meV, (the shifts are seen from 120 meV to 220 meV) corresponding to band bending of the same amount. For the 100 nm Ag point we were unable to accurately measure the Ti 2p binding energy, as the Ti signal was attenuated by the high Ag surface coverage. Based on these results we suggest that the band bending of the TiO_2|Ag system is at least 170 meV or greater, since it is probable the band bending continued to increase with further Ag deposition but could not be measured here. Given that the measured V_{oc} in Schottky barrier solar cells is limited by the barrier height we can use the J-V measurements to ascertain the band bending for higher Ag thickness cells. The 10 nm Ag solar cells exhibit a V_{oc} of ~160 mV, in agreement with the band bending we measure. Moreover, the 100 nm Ag solar cells show a higher V_{oc} of ~350-400 mV that support the CREM work function measurements, which show an increase of 480 meV.

Overall the energy band alignment, including the band bending for the TiO_2|Ag solar cells, based on the CREM is in favor of formation of a Schottky barrier between the rough TiO_2 and the nanostructured Ag film (Figure 7c). The Ag, which is directly deposited by sputtering on the rough TiO_2 surface, plays a triple role in TiO_2|Ag solar cells. First, the Ag forms a schottky barrier with the TiO_2. Second, the Ag performs as the back contact material for the solid state TiO_2|Ag devices, conducting the holes formed in the solar cells to the electrical contacts. Third,

the Ag nanoparticles absorb the incoming light by exciting SPR. The SPR then decays to its original ground state and on the way it excites 'hot' non equilibrium electrons that can be injected into the TiO_2, producing photocurrent and photovoltaic activity. 'Hot' electron injection into the TiO_2 was reported to be very fast, occurring within 50 fs of their formation, for gold nanoparticles without a hole transport layer.[29] The formation of 'hot' electrons in silver nanoparticles is very fast and is on the order of less than 30 fs,[30] whereas electron-electron scattering and thermalization occur in approximately 100 fs.[5] From the reported timescales, we suggest that in our solar cells, which contain no hole transport layer, the 'hot' electron injection from the Ag into the TiO_2 happens on time scales between 30 to 100 fs. The addition of the hole transport material may further improve our TiO_2|Ag solar cells, and help decrease injection times, while preventing the recombination of 'hot' electrons in the Ag with oxidized silver atoms that are close to them.

3. Conclusion

In this research, we have demonstrated a simple and direct method for forming TiO_2|Ag independent plasmonic solar cells. The silver was deposited by sputtering, with varying durations, on a rough TiO_2 surface, forming a Schottky junction between the two. The use of sputtering has advantages like controlled deposition times and the removal of complicated templating techniques to form the Ag nanoparticles. The Ag was shown to form metallic nanoparticles, which indicates that it has plasmonic absorptions that lead to SPR. The decay of the SPR excites non-equilibrium electrons, known as 'hot' electrons in the Ag, which are injected into the TiO_2, producing photocurrent. The observed photovoltaic activity is high, with the best solar cells reaching efficiencies of 0.2%, which to our knowledge have not been

achieved so far for this type of solar cell. The source of the 'hot' electrons is the wide IPCE active band (390 nm-700 nm) of the Ag nanoparticles, which have a large size distribution, contributing to the wide plasmonic absorption. XPS-based CREM confirms the injection of 'hot' electrons from the Ag into the TiO_2, further proving the 'hot' electron mechanism. The Ag has three roles on our solar cells, first, as the metal forming the Schottky barrier with the TiO_2 semiconductor. Second, as the back contact material conducting holes away from the TiO_2 leading to charge separation, and third, most important role, as the material forming the 'hot' electrons that are injected into the TiO_2, generating photovoltaic activity. The relatively high photovoltaic activity that we see may suggest that a large size distribution of metallic nanoparticles for photovoltaic devices is better than the commonly used homogeneous size distribution.

4. Experimental Section

Library preparation

Synthesis of TiO_2 layer: The TiO_2 thin film layer was deposited by a home-built spray pyrolysis system[31] on a commercially available fluorine doped tin oxide (FTO) coated glass substrate, TEC 15 (72 mm x 72 mm, Hartford Glass Co., Inc.). The glass substrate was cleaned in a sonication bath with soap and deionized water then rinsed in dry ethanol, and washed again with deionized water. The substrate was then treated with Ar plasma for 5 minutes (PLASMA-PREEN II-862, Plasmatic Systems, Inc.). The glass substrate was placed on a preheated hotplate (Harry Gestigkeit GmbH) heated to 450 °C. The spray pyrolysis system set-up consists of a 3-axis CNC robot (EAS GmbH), a Sono-tek 120 KHz ultrasonic spraying nozzle, and a syringe pump (New Era Pump Systems, Inc.) for pumping the precursor solution. The TiO_2 precursor

solution was prepared by mixing 7.5 ml of titaniumtetraisopropoxide (TTiP, Sigma-Aldrich) and 5 ml of acetylacetone (Sigma-Aldrich) in 240 ml of ethanol (Carlo Erba Reagents), and its pH was 6.8. The precursor carrier gas was filtered dry clean air, and the flow rate was kept at 60 ml hr^{-1}. The precursor solution was sprayed using a program that was set to form a linear thickness gradient of the TiO_2 layer, with thicknesses varying from 165 to 440 nm (Figure S5a, Supporting Information).

Deposition of Ag layer: The silver nanostructured thin films were prepared by RF magnetron sputtering (AJA International Inc.). To deposit the Ag, a shadow-mask with an array of 13 x 13 round holes with a diameter of 1.8 mm, was placed on the substrate with the TiO_2 layer. The sputtering system was pumped down to a base pressure of 1.4×10^{-7} torr. The silver was deposited from a 2" Ag target (99.99%, Testbourne Ltd) under Ar gas at a flow rate of 30 sccm, and the total pressure in the chamber was 2 mtorr. The target power was kept at 100 W, and the substrate temperature was 23 °C. The deposition time and calibrated Ag thicknesses (**Table 1**) were calculated based on a deposition rate of 2.4 Å s^{-1}, which was measured by a quartz microbalance. In order to deposit the silver thickness gradient, each row of the shadow-mask (Figure 2) was exposed separately for different sputtering times, as shown in table 1. The deposited Ag thicknesses varied from 5 to 160 nm.

Row	1	2	3	4	5	6	7	8	9	10	11	12	13
Deposition time (s)	20	40	60	80	120	160	200	240	320	400	480	560	640
Ag thickness (nm)	5	10	15	20	30	40	50	60	80	100	120	140	160
XPS		*								*			
SEM & particle size analysis			*		*				*		*		
IPCE					*	*	*	*	*	*	*	*	*

Table 1. Sputtering deposition time and estimated Ag thickness for each row of the library, the library structure is shown in Figure 2. The Ag points that were analyzed beyond the typical J-V characterizations are marked in the table as well.

Material characterization

Morphology and surface structuring of TiO_2 and A: The surfaces of the bare TiO_2 and of the TiO_2 coated with Ag were characterized by a field-emission Helios 600 high resolution scanning electron microscope (HRSEM, FEI). The energy-dispersive X-ray analysis (EDS) in the HRSEM was executed by an 80 mm^2 X-max detector (Oxford Instruments). Cross section images of the TiO_2|Ag library were taken using a Focused Ion Beam Helios 600 scanning electron microscope system (FEI). Images were taken for points with Ag deposition times of 60 s and 480 s.

Chemical and electrical analysis: X-ray photoelectron spectroscopy (XPS) and chemically resolved electrical measurements (CREM)[26b, 32] were performed using a Kratos AXIS-Ultra-DLD spectrometer, with a monochromated Al kα x-ray source, applied at low power values, 15-75 W. Core level spectra, work functions, and valence band onsets were measured at selected points on the library with Ag thicknesses of 10 and 100 nm. A bare TiO_2 reference sample was measured as well. The stability of samples under the x-ray irradiation was continuously followed, including minor charging effects. Electrical properties of the samples were further investigated by applying light illumination, using a 250 W halogen lamp at 3200 K (KL 1500 LCD, SCHOTT), equipped with a set of low-pass filters. All measurements correspond to long timescales, on the order of 100-1000 seconds.

Solar cell device characterization

Solar cell current density- voltage (J-V) characterization: The J–V characteristics of 169 solar cells were measured with a home-built automated scanning J–V system described in depth in our previous reports.[6a, 21] In order to make an electrical contact to the FTO, a metal frame was ultrasonically soldered around the library edges. The library was illuminated using a xenon laser-driven light source (LDLS, EQ-99FC, ENERGETIQ), which was calibrated to the emission of AM1.5G. The source meter for the J-V electrical measurements was a Keithley 2400. The J–V curve was measured twice, in ascending and descending scan directions, for all the points. The ascending and descending measurements were made to eliminate cells with excessive capacitance. Solar cells that had a less than a 15% difference between the ascending and descending were defined as photovoltaic, and the rest of the points are not analyzed or discussed in this work.

Quantum efficiency measurements (IPCE): IPCE measurements were carried out on a Solar Cell Quantum Efficiency Measurement System (Model QEX10, PV Measurements Inc.). The IPCE was measured in AC mode with a bias halogen white light. The IPCE calibration was performed using a slandered certified Si photodiode. The Chopper frequency was set to 4 Hz, and the perturbing light was a monochromatic Xe lamp. The measurement range was between 350 to 1000 nm, and the measurement step was 5 nm. The center column on the library (same TiO_2 thickness, Figure 2) was measured, in order to see the dependence of the IPCE on the Ag thickness.

Supporting Information

Supporting Information is available from the Wiley Online Library or from the author.

Acknowledgements

The research was supported by the Israeli National Nanotechnology Initiative (INNI, FTA project), and by the European Union's Seventh Program for research, technological development and demonstration under grant agreement no. 309018. H.N.B. would like to thank the Israeli Ministry of Science, Technology, and Space for their financial support. The authors would like to thank Dr. Olga Girshevitz, Israel, for the RBS measurements. The authors would also like to thank Dr. Kate Gotlib-Vainshtein, from the Bar Ilan Institute for Nanotechnology and Advanced Materials, for her help with the HRSEM measurements.

Received: ((will be filled in by the editorial staff))
Revised: ((will be filled in by the editorial staff))
Published online: ((will be filled in by the editorial staff))

[1] S. Linic, P. Christopher, D. B. Ingram, Nat. Mater. **2011**, *10*, 911.
[2] H. A. Atwater, A. Polman, Nat. Mater. **2010**, *9*, 205.
[3] H. Fang, C. X. Zhang, L. Liu, Y. M. Zhao, H. J. Xu, Biosens. Bioelectron. **2015**, *64*, 434.
[4] a) A. Özkan, M. H. Özkan, R. Gürkan, M. Akçay, M. Sökmen, J. Photochem. Photobiol. A **2004**, *163*, 29; b) D. Sarkar, C. K. Ghosh, S. Mukherjee, K. K. Chattopadhyay, ACS Appl. Mater. Interfaces **2013**, *5*, 331.
[5] C. Clavero, Nat. Photonics **2014**, *8*, 95.
[6] a) S. Rühle, H. N. Barad, Y. Bouhadana, D. A. Keller, A. Ginsburg, K. Shimanovich, K. Majhi, R. Lovrincic, A. Y. Anderson, A. Zaban, Phys. Chem. Chem. Phys. **2014**, *16*, 7066; b) T. Hirakawa, P. V. Kamat, Langmuir **2004**, *20*, 5645; c) B. Kupfer, K. Majhi, D. A. Keller, Y. Bouhadana, S. Rühle, H. N. Barad, A. Y. Anderson, A. Zaban, Adv. Energy Mater. **2015**, *5*, 1401007.
[7] S. T. Kochuveedu, Y. H. Jang, D. H. Kim, Chem. Soc. Rev. **2013**, *42*, 8467.
[8] a) Y. Takahashi, T. Tatsuma, Nanoscale **2010**, *2*, 1494; b) E. Kazuma, N. Sakai, T. Tatsuma, Chem. Commun. **2011**, *47*, 5777; c) Q. Gan, F. J. Bartoli, Z. H. Kafafi, Adv. Mater. **2013**, *25*, 2385.
[9] Q. Lu, Z. Lu, Y. Lu, L. Lv, Y. Ning, H. Yu, Y. Hou, Y. Yin, Nano Lett. **2013**, *13*, 5698.
[10] a) J. Yun, S. H. Hwang, J. Jang, ACS Appl. Mater. Interfaces **2015**, *7*, 2055; b) H. Dong, Z. Wu, Y. Gao, A. El-Shafei, S. Ning, J. Xi, B. Jiao, X. Hou, Org. Electron. **2014**, *15*, 2847; c) H.-Y. Kim, D. H. Song, H. Yoon, J. S. Suh, RSC Adv. **2015**, *5*, 27464.
[11] a) M. B. Rajendra Prasad, S. Deena, C. Rajesh, V. K. Pandit, H. M. Pathan, J. Renewable Sustainable Energy **2013**, *5*, 031615; b) K. Guo, Z. Liu, J. Han, X. Zhang, Y. Li, T. Hong, C. Zhou, J. Power Sources **2015**, *285*, 185.
[12] K. Liu, Y. Bi, S. Qu, F. Tan, D. Chi, S. Lu, Y. Li, Y. Kou, Z. Wang, Nanoscale **2014**, *6*, 6180.
[13] Y. Tian, T. Tatsuma, Chem. Commun. **2004**, 1810.
[14] W. Li, F. Chen, J. Alloys Compd. **2015**, *632*, 845.
[15] L. S. Daniel, H. Nagai, M. Sato, J. Mater. Sci. **2013**, *48*, 7162.
[16] C. Gunawan, W. Y. Teoh, C. P. Marquis, J. Lifia, R. Amal, Small **2009**, *5*, 341.
[17] Y. Takahashi, T. Tatsuma, Appl. Phys. Lett. **2011**, *99*, 182110.
[18] P. Reineck, G. P. Lee, D. Brick, M. Karg, P. Mulvaney, U. Bach, Adv. Mater. **2012**, *24*, 4750.
[19] I. Takeuchi, J. Lauterbach, M. J. Fasolka, Mater. Today **2005**, *8*, 18.
[20] S. Rühle, A. Y. Anderson, H. N. Barad, B. Kupfer, Y. Bouhadana, E. Rosh-Hodesh, A. Zaban, J. Phys. Chem. Lett. **2012**, *3*, 3755.
[21] A. Y. Anderson, Y. Bouhadana, H. N. Barad, B. Kupfer, E. Rosh-Hodesh, H. Aviv, Y. R. Tischler, S. Rühle, A. Zaban, ACS Comb. Sci. **2014**, *16*, 53.
[22] I. T. Chashechnikova, V. M. Vorotyntsev, V. V. Borovik, G. I. Golodets, I. V. Plyuto, A. P. Shpak, Theor. Exp. Chem. **1992**, *28*, 216.
[23] J. Morales, L. Sánchez, F. Martín, J. R. Ramos-Barrado, M. Sánchez, J. Electrochem. Soc. **2004**, *151*, A151.
[24] R. Gottesman, S. Tirosh, H.-N. Barad, A. Zaban, J. Phys. Chem. Lett. **2013**, *4*, 2822.
[25] J. Bonsak, J. Mayandi, A. Thøgersen, E. Stensrud Marstein, U. Mahalingam, Phys. Status Solidi C **2011**, *8*, 924.
[26] a) Y. Itzhaik, G. Hodes, H. Cohen, J. Phys. Chem. Lett. **2011**, *2*, 2872; b) H. Cohen, Appl. Phys. Lett. **2004**, *85*, 1271.

[27] R. Buller, H. Cohen, E. Minkin, R. Popovitz-Biro, E. Lifshitz, M. Lahav, Adv. Funct. Mater. **2002**, *12*, 713.
[28] V. Pfeifer, P. Erhart, S. Li, K. Rachut, J. Morasch, J. Brötz, P. Reckers, T. Mayer, S. Rühle, A. Zaban, I. Mora Seró, J. Bisquert, W. Jaegermann, A. Klein, J. Phys. Chem. Lett. **2013**, *4*, 4182.
[29] L. Du, A. Furube, K. Hara, R. Katoh, M. Tachiya, J. Photochem. Photobiol. C **2013**, *15*, 21.
[30] C. Voisin, D. Christofilos, N. D. Fatti, F. Vallee, Eur. Phys. J. D **2001**, *16*, 139.
[31] M. Pavan, S. Rühle, A. Ginsburg, D. A. Keller, H. N. Barad, P. M. Sberna, D. Nunes, R. Martins, A. Y. Anderson, A. Zaban, E. Fortunato, Sol. Energy Mater. Sol. Cells **2015**, *132*, 549.
[32] I. Doron-Mor, A. Hatzor, A. Vaskevich, T. van der Boom-Moav, A. Shanzer, I. Rubinstein, H. Cohen, Nat. **2000**, *406*, 382.

TiO_2|Ag solid state plasmonic solar cells are shown to give efficiencies of 0.2%, which is high for these types of cells. The Ag is sputtered directly on to the TiO_2, which has a rough surface, enabling formation of Ag nanoparticles. Quantum efficiency measurements and electrical and analysis reveal that the 'hot' electron mechanism is responsible for the photovoltaic activity.

Hannah-Noa Barad, Adam Ginsburg, Hagai Cohen, Kevin J. Rietwyk, David A. Keller, Shay Tirosh, Yaniv Bouhadana, Assaf Y. Anderson,* and Arie Zaban*

Hot Electron Based Solid State TiO_2|Ag solar cells

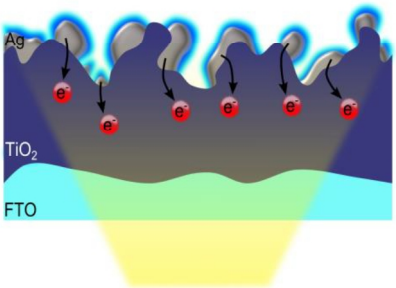

Supporting Information

Hot Electron Based Solid State TiO_2|Ag solar cells

Hannah-Noa Barad, Adam Ginsburg, Hagai Cohen, Kevin J. Rietwyk, David A. Keller, Shay Tirosh, Yaniv Bouhadana, Assaf Y. Anderson, and Arie Zaban**

RBS analysis

RBS measurements were performed using a 1.7MV Pelletron accelerator from NEC. The RBS (Rutherford Backscattering) spectrum was obtained with a fixed silicon drift detector (ULTRATM Silicon-Charged Particle Detector, ORTEC) in Cornell geometry. The beam used for collecting the spectrum was a 2.022 MeV $4He^{++}$ 1Kev beam. The beam diameter was 1.5 mm, with a beam current of ~10 nA. The RBS Fixed detector scattering angle, Θ, was 169° (Cornell geometry), solid angle, Ω, was 2.7 msr, and a Be window 125 µm thick with a 5 µm thick Mylar filter was used to stop $4He^{+}$ ions at 2.023 MeV. An integrated charge (Q) of 10 µC was used for all measurements. RBS Spectrum analysis was done using the Surrey IBA DataFurnace software.[1]

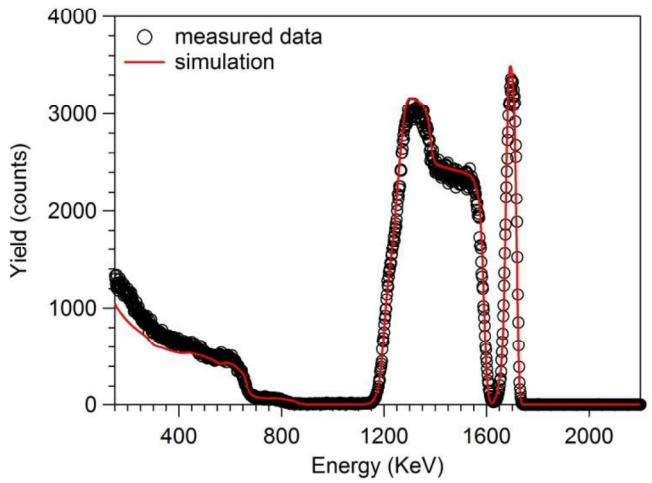

Figure S1. RBS measurements of the TiO_2/Ag library. The sharp peak at the energy of ~1700 KeV is the surface peak of the silver. The broad peak to the left is the Sn arising from the FTO layer, on top of which the Ti peak appears as well. From the fit analysis, which helps quantify the concentration of the elements in each layer, it was determined that the surface peak contains 100 % Ag atoms, meaning that metallic Ag is produced. The sharp Ag peak and lack of overlap

between the Ag peak and the Sn and Ti peaks indicate that the silver is on the surface of the TiO_2 and that no intermixing or formation of silver oxides is present.

EDS analysis

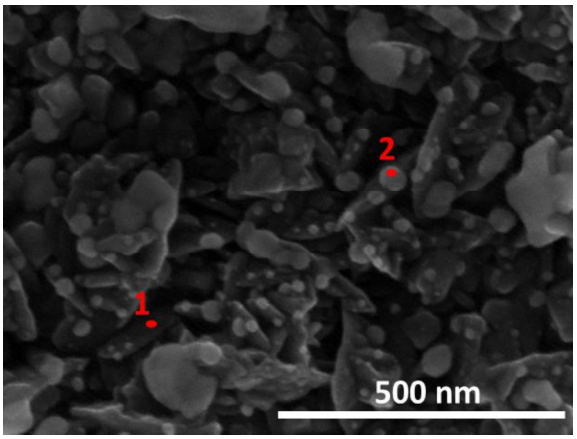

Figure S2. SEM Image of two points measured by EDS analysis. **1.** Bare TiO_2 area, and **2.** Ag nanoparticle area.

Element	Atomic percentage	
	point 1	**point 2**
C K	6.44	6.15
Si K	0.28	0.21
Ti K	18.83	20.36
Ag L	-	2.36
Sn L	7.79	5.43
O	66.67	65.49

Table S1. Atomic percentages of the elements detected by EDS for two different points on the sample as indicated by Figure S2. The first point shows that there is no Ag in that area, indicating bare TiO_2, and the second point shows a small amount of Ag, indicating that the silver is deposited and nanoparticles and nanostructures on the surface of the TiO_2, leaving some areas of TiO_2 uncovered.

Silver nanoparticle size analysis

Silver nanoparticle sizes were analyzed by image processing, using ImageJ software (Image Processing and Analysis in Java, NIH). An HRSEM image of the silver nanoparticles on TiO_2 was loaded onto the program for analysis. The image scale was calibrated to 400 nm, and the threshold was set to 140-225. The particle analysis size was set to different ranges (10-100, 100-3000, 10000-25000, and 25000-50000 cm^2) in order to differentiate between and correctly analyze the very small Ag nanoparticles and the larger Ag nanostructures. The particle diameter was calculated using Feret's diameter, which is a projection of a 3D image into a 2D plane. The achieved Ag particle size distribution was analyzed and plotted on a histogram using IGOR Pro (WaveMetrics, Inc.). The particles' volumes were calculated based on the diameter.

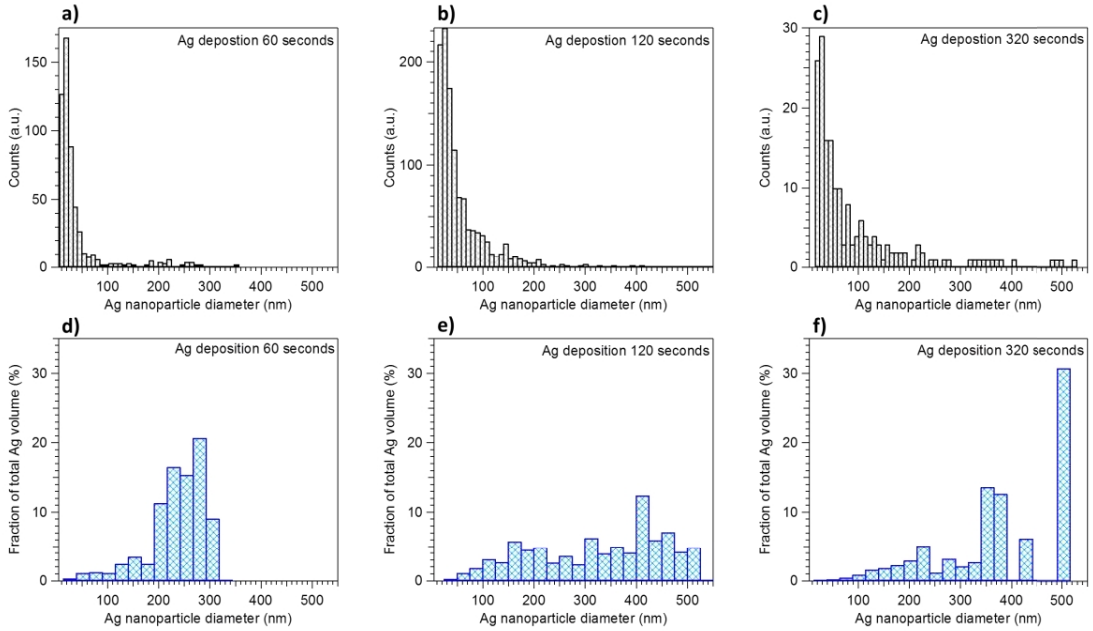

Figure S3. Silver particle size distribution analysis. a-c) particle diameter distributions of 60 s, 120 s, and 320 s Ag deposition times. d-f) Ag volume fraction of total Ag volume as a function of particle diameters, for 60 s, 120 s, and 320 s Ag deposition times. The small silver nanoparticles have diameters that are smaller than 5, while the larger Ag nanopaticles reach sizes

up to ~500 nm. The nanoparticle sizes vary depending on the Ag deposition time. As the Ag deposition time increases the sizes of the nanoparticles become much larger, and most of the Ag volume is concentrated in the large nanoparticles. The large size variation of the nanoparticles within the same deposition time is the reason for the wide IPCE absorption seen from 390 nm to 700 nm. The shift in the position of the IPCE peak is caused by the general shift to larger sizes of nanoparticles with higher deposition times.

Energy band alignment by XPS

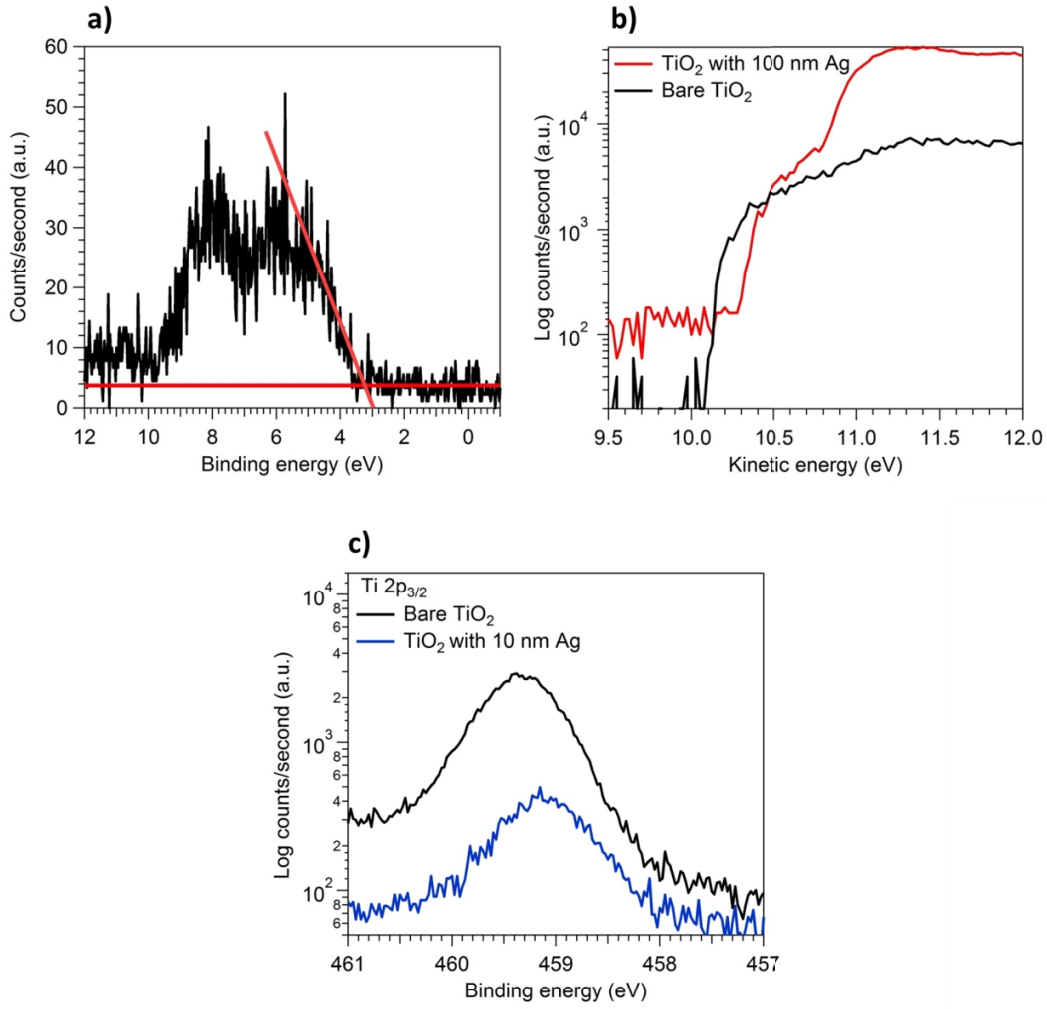

Figure S4. a) XPS valence measurements: the valence band maximum is determined by the crossing of two linear lines, one that established the background and the other is the onset of the valence band. The valence band maximum is extracted from the x-axis juncture of a linear line going through the crossing. It is important to note that there was a charging on the sample of ~330 meV to the left, and consequently the valence band maximum was corrected and measured to be 3.25 eV **b)** XPS Low energy electron cut-off measurements were used to find the work functions of the bare TiO_2 and the TiO_2 coated with 100 nm of Ag. The work function is ascertained from the intercept between the x-axis and a linear fit to the onset. **c)** XPS measurement of Ti $2p_{3/2}$ core level peaks, for bare TiO_2 and TiO_2 coated with 10 nm of Ag. There is a shift of ~120-220 meV between the bare TiO_2 and the TiO_2 coated with 10 nm of Ag. This shift correlates with the TiO_2 band bending that occurs when Ag is added on top of the TiO_2, and is also supported by the V_{oc} values that are observed.

TiO_2 bandgap and thickness calculations

Bandgap calculations: Optical measurements of total transmission (TT) total reflection (TR) and specular reflections (SR) were measured for the TiO_2 layer, using a home built optical scanner reported elseware.[2] The TiO_2 absorptance (A) was calculated as: $A= 1-TT-TR$

The absorption coefficient (α) was calculated based on the absorptance as: $\alpha= (-\ln(1-A))/d$

Where d is the TiO_2 thickness at a given point. The absorption coefficient was then used to prepare Tauc plots, which were linearly fitted to the x-axis intercept, and the bandgap was extracted from the intercept point.

TiO_2 thickness calculations: The thickness of the TiO_2 layer was calculated using a commercially available optical modeling software (CODE).[3] The modeling software takes the

TT and SR measurements and simulates spectra to fit them. The simulations are based on the OJL interband transition model.

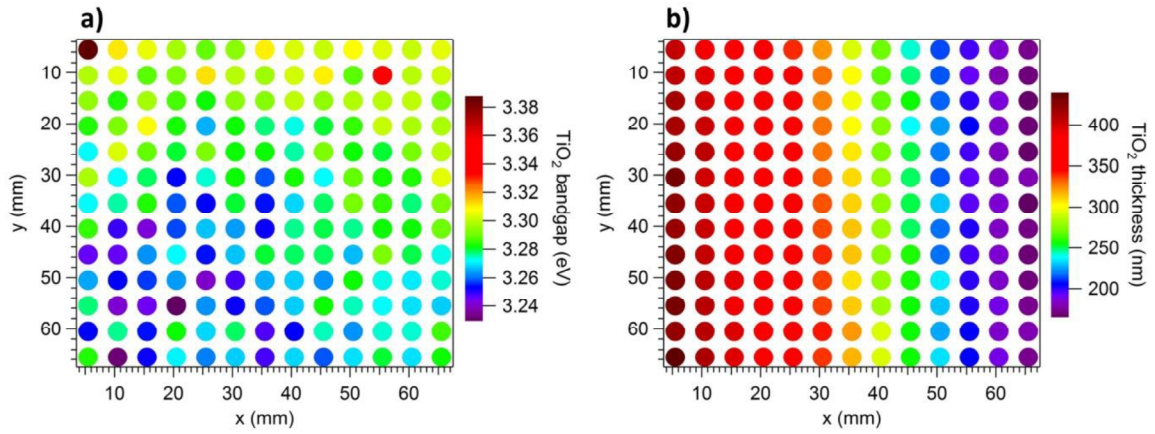

Figure S5: a) TiO_2 map of bandgaps calculated for the library. The average bandgap value that was calculated was 3.26 eV. **b)** Thickness map of TiO_2 on the library, calculated from the optical measurements. The TiO_2 has a linear thickness gradient, with the highest thicknesses on the left side of the library (440 nm) and the lowest thickness of the TiO_2 on the right side of the library (160 nm).

References:

[1] C. Jeynes, N. P. Barradas, P. K. Marriott, G. Boudreault, M. Jenkin, E. Wendler, R. P. Webb, J. Phys. D: Appl. Phys. 2003, 36, R97.

[2] A. Y. Anderson, Y. Bouhadana, H. N. Barad, B. Kupfer, E. Rosh-Hodesh, H. Aviv, Y. R. Tischler, S. Rühle, A. Zaban, ACS Comb. Sci. 2014, 16, 53.

[3] D. A. Keller, A. Ginsburg, H. N. Barad, K. Shimanovich, Y. Bouhadana, E. Rosh-Hodesh, I. Takeuchi, H. Aviv, Y. R. Tischler, A. Y. Anderson, A. Zaban, ACS Comb. Sci. 2015, 17, 209.